Experimental Response and Damage of SC-CLT Shear Walls under Multidirectional Cyclic Lateral Loading

Alia Amer, Ph.D., A.M.ASCE[1]; Richard Sause, Ph.D., P.E., M.ASCE[2]; and James Ricles, Ph.D., P.E., M.ASCE[3]

Abstract: This paper presents an experimental study on the multidirectional cyclic lateral-load response of post-tensioned self-centering (SC) cross-laminated timber (CLT) shear walls. SC-CLT shear wall damage states are introduced and qualitatively defined in terms of the repairs needed to restore the lateral-load response of the SC-CLT wall. A comparison between SC-CLT wall damage states under unidirectional (in-plane) and multidirectional (in-plane and out-of-plane) lateral loading is presented. The experimental results show that the initiation of SC-CLT wall damage occurs at smaller story drifts under multidirectional loading compared to unidirectional loading. Engineering demand parameters (EDPs) are used to quantify the SC-CLT wall damage states. Uncertainty in the EDP value when a damage state occurs is considered and quantified. Using the experimental results, component (i.e., a CLT wall panel corner) and system (i.e., an entire SC-CLT wall) fragility functions are developed and presented. **DOI: 10.1061/JSENDH.STENG-12576.**

Author keywords: Cross-laminated timber (CLT); Self-centering (SC); Multidirectional lateral loading; Lateral-load response; Damage states; Repair; Fragility functions; Earthquake performance.

Introduction

Cross-laminated timber (CLT) panels are engineered wood structural components fabricated by laminating layers of timber boards in an orthogonal pattern, where the boards are glued together on their wide faces and not edge-glued. Low-damage post-tensioned (PT) self-centering (SC) CLT shear walls (SC-CLT walls) provide an opportunity to develop seismically resilient CLT buildings (Akbas et al. 2017; Ganey et al. 2017; Pei et al. 2019). An SC-CLT wall is designed for gap opening of the joint between the base of the CLT wall panels and the foundation when the overturning moment from lateral forces is large enough to overcome the precompression from the post-tensioning, leading to a controlled-rocking response [Fig. 1(a)].

Previous research focused primarily on the lateral-load response of isolated self-centering timber walls without considering the interaction with the adjacent floor diaphragms, collector beams, and gravity load system. Extensive research on post-tensioned controlled-rocking timber walls under *unidirectional* loading has been conducted (Palermo et al. 2006; Dunbar et al. 2014; Iqbal et al. 2015). Moroder et al. (2017) investigated deformation incompatibilities between post-tensioned controlled-rocking laminated veneer lumber (LVL) walls and collector beams under *unidirectional* loading and considered various collector-beam-to-rocking-wall connections to transfer the lateral forces to the walls. Experimental and analytical studies on the lateral-load response under unidirectional loading of single-panel SC-CLT walls and multipanel SC-CLT walls coupled with U-shaped flexural plates (UFPs) have been conducted (Akbas et al. 2017; Ganey et al. 2017). Full-scale tests of a 2-story mass-timber building with SC-CLT walls using *unidirectional* strong ground motions were performed by Pei et al. (2019) on the University of California, San Diego (UCSD) [Natural Hazards Engineering Research Infrastructure (NHERI) at UCSD] shake table. Because *multidirectional* loading is likely to be more damaging to SC-CLT wall panels than *unidirectional* loading, there are concerns about the seismic resilience of buildings under *multidirectional* loading, and better understanding of the lateral-load response and damage states of SC-CLT walls under *multidirectional* loading is needed.

This paper presents the lateral-load response of SC-CLT walls from experiments on a 0.625-scale timber test subassembly under cyclic loading. Comparisons are made between the lateral-load responses of SC-CLT walls from a unidirectional test (UT) and a multidirectional test (MT). Based on visual observations, SC-CLT wall damage states are introduced and are qualitatively defined in terms of repairs needed to restore the lateral-load response of the wall. Three engineering demand parameters (EDPs) are considered to quantify the SC-CLT wall damage states: (1) the floor (diaphragm) story drift; (2) the SC-CLT wall story drift; and (3) the CLT wall panel corner compression strain. Fragility functions are developed from the experimental results. The experimental results are valuable for calibrating numerical models for seismic performance prediction of SC-CLT wall buildings. The fragility functions are a valuable resource for assessing the potential damage to SC-CLT walls under unidirectional and multidirectional seismic loading.

[1]Postdoctoral Research Associate, ATLSS Engineering Research Center, Dept. of Civil and Environmental Engineering, Lehigh Univ., Bethlehem, PA 18015 (corresponding author). Email: ama616@lehigh.edu

[2]Joseph T. Stuart Professor of Structural Engineering, ATLSS Engineering Research Center, Dept. of Civil and Environmental Engineering, Lehigh Univ., Bethlehem, PA 18015. ORCID: https://orcid.org/0000-0002-6143-4385. Email: rs0c@lehigh.edu

[3]Bruce G. Johnston Professor of Structural Engineering, ATLSS Engineering Research Center, Dept. of Civil and Environmental Engineering, Lehigh Univ., Bethlehem, PA 18015. Email: jmr5@lehigh.edu

Note. This manuscript was submitted on March 15, 2023; approved on July 5, 2023; published online on November 20, 2023. Discussion period open until April 20, 2024; separate discussions must be submitted for individual papers. This paper is part of the ***Journal of Structural Engineering***, © ASCE, ISSN 0733-9445.

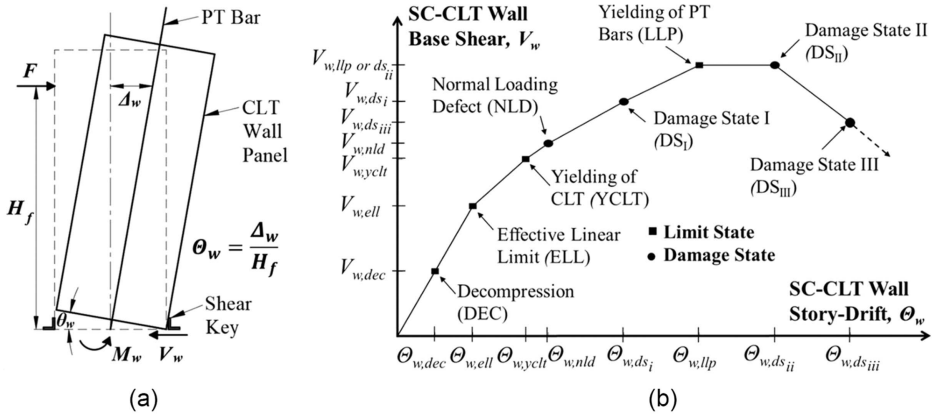

Fig. 1. (a) Controlled-rocking lateral-load response of single-panel SC-CLT wall; and (b) SC-CLT wall base shear versus story drift response with structural limit states and damage states identified.

Structural Limit States and Damage States of SC-CLT Wall Lateral-Load Response

The lateral-load response of SC-CLT walls is governed by shear and flexural deformation of the CLT wall panels, and controlled rocking of the panels on the foundation [Fig. 1(a)]. A series of structural limit states and damage states are used to characterize the lateral-load response of SC-CLT walls. The idealized SC-CLT wall base shear V_w versus SC-CLT wall story drift Θ_w response is shown in Fig. 1(b), which identifies the structural limit states and the initiation of damage states for a single-panel SC-CLT wall. The Θ_w is the lateral-relative displacement at the floor level, denoted Δ_w, divided by the story height H_f and is given in percent (%) radians. The initiation of a damage state is defined as the first occurrence of a visible damage form, described subsequently in detail, at a corner of the wall panel in compression at the base of the wall [e.g., the right edge in Fig. 1(a)].

The SC-CLT wall structural limit states are based on local compression stress and strain at the base of the CLT wall panel, and the PT bar force (Kurama et al. 1999a, b; Perez et al. 2007; Akbas et al. 2017; Ganey et al. 2017). The structural limit states include (1) decompression of the base of the wall (DEC); (2) effective limit of the linear-elastic response of the wall [effective linear limit (ELL)]; (3) yielding of the composite CLT material (YCLT) at the CLT wall panel corner; and (4) yielding of the PT bars (LLP).

The SC-CLT wall damage states are defined qualitatively in terms of repair actions. The objective of the repair should be to restore the exterior finish of the CLT wall panels and/or restore the lateral-load response of the SC-CLT wall (i.e., restore the stiffness and strength characteristics of the lateral-load response). Table 1 summarizes the different damage states with the damage forms observed experimentally and the possible repair actions. An identifier is associated with the damage state and observed damage form, for example, NLD-a is the normal loading defect damage state where fine compression splits at the wall corner are observed. Four damage states are considered: (1) normal loading defect (NLD); (2) Damage State I (DS$_I$); (3) Damage State II (DS$_{II}$); and (4) Damage State III (DS$_{III}$). NLD, DS$_I$, and DS$_{II}$ are local damage states and DS$_{III}$ is a global damage state.

Fig. 2 shows the stress and strain distribution, along with internal forces at the base of a single-panel SC-CLT wall at various damage states, where L_w is the wall panel length, C is the compression

Table 1. SC-CLT wall damage states and possible repair actions

Identifier	Damage state	Damage form	Possible repair action
NLD-a	NLD	Fine compression splits	No repair needed
NLD-b	NLD	Wrinkling	No repair needed
DS$_I$-a	DS$_I$	Initiation of outer-ply delamination and/or buckling	Reglue delaminated layers
DS$_I$-b	DS$_I$	Initiation of corner rounding	Replace damaged ply[a]
DS$_I$-c	DS$_I$	Initiation of localized corner crushing	Replace damaged ply[a]
DS$_{II}$-a	DS$_{II}$	Excessive outer-ply delamination and/or buckling	Add steel-plate reinforcement to CLT wall panel or CLT wall panel replacement
DS$_{II}$-b	DS$_{II}$	Excessive corner rounding	Add steel-plate reinforcement to CLT wall panel or CLT wall panel replacement
DS$_{II}$-c	DS$_{II}$	Excessive localized corner crushing	Add steel-plate reinforcement to CLT wall panel or CLT wall panel replacement
DS$_{II}$-d	DS$_{II}$	Excessive end rolling	Add steel-plate reinforcement to CLT wall panel or CLT wall panel replacement
DS$_{III}$[b]	DS$_{III}$	20% degradation in base shear resistance	CLT wall panel replacement

[a]Possible repair action was not tested.
[b]Damage state is not based on specific visible damage.

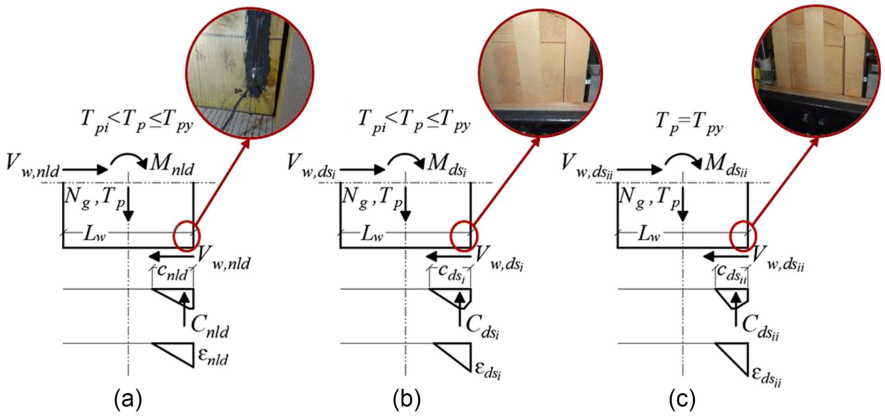

Fig. 2. Stress and strain at base of single-panel SC-CLT wall at damage states: (a) NLD in form of fine compression splits; (b) DS_I in form of initiation of outer ply delamination; and (c) DS_{II} in form of excessive outer ply delamination and buckling.

force at the base of the CLT wall panel, c is the contact length with the foundation, ε is the local compression strain at the CLT wall panel corner, T_{pi} is the initial PT bar force, T_{py} is the PT bar force at PT bar yielding, N_g is the gravity force, and M is the overturning moment. The subscripts in the notation of Fig. 2 represent a damage state (e.g., C_{dsi} is the compression force at DS_I). The local damage states are based on visual observations of the test results and are associated with values of ε, denoted ε_{nld}, ε_{dsi}, and ε_{dsii}, for NLD, DS_I, and DS_{II}, respectively, as shown in Fig. 2. The global damage state (DS_{III}) is based on the lateral-load response observed in the test results and the associated ε value is undefined.

As summarized in Table 1, NLD is indistinguishable minor or cosmetic damage of the CLT wall panel [Fig. 2(a)] that can be caused by lateral loading, gravity loading, or timber shrinkage. NLD does not require any repair action. DS_I is a moderate damage state [Fig. 2(b)], where a decrease in the base shear resistance of the wall is expected to be negligible, and a cosmetic repair is needed (Table 1). DS_{II} is a significant damage state [Fig. 2(c)] where a decrease in the lateral stiffness and/or strength of the wall is expected to occur. Following the initiation of DS_{II}, repair and/or strengthening of the CLT wall panel [e.g., adding steel-plate reinforcement to the damaged CLT wall panels (Amer 2023)] or replacement of the CLT wall panels is required. The occurrence of NLD is dependent on the CLT panel wood species and the design of the SC-CLT wall, and it may occur before, coincide with, or occur after the YCLT limit state is reached. DS_I and DS_{II} occur after the YCLT limit state is reached. The expected PT bar force T_p at each local damage state is shown in Fig. 2. DS_{III} is both a structural limit state and a damage state. DS_{III} is a severe damage state where the CLT wall panels are damaged to the extent that a 20% reduction in base shear resistance of the SC-CLT wall occurs. DS_{III} is considered to be the failure state and is consistent with failure of other types of structural walls (e.g., ACI 2007). DS_{III} is not based on a visible damage and the associated ε value is unknown. The CLT wall panels should be replaced after DS_{III} has been reached.

Description of Lateral Loading Tests

Test Subassembly and SC-CLT Wall Details

The 0.625-scale timber test subassembly, shown in Fig. 3, represents part of a prototype SC-CLT shear wall building. The overall dimensions of the test subassembly were selected to fit laboratory constraints. The test subassembly consists of an SC-CLT wall,

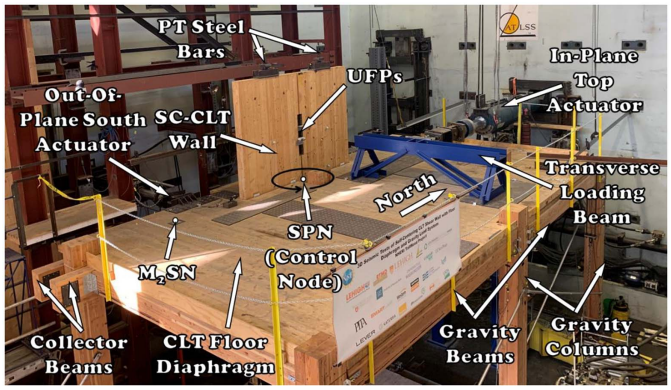

Fig. 3. Isometric view of 0.625-scale test subassembly.

a CLT floor diaphragm, glulam collector beams, and a glulam gravity load system (Sause et al. 2020; Amer 2023). The CLT panels were provided by SmartLam (Columbia Falls, Montana) (APA—The Engineered Wood Association 2016) and certified as Grade SL-V4 based on standard PRG 320 (APA—The Engineered Wood Association 2019) for CLT panels. The panels were Spruce-Pine-Fir South (SPF-S) CLT. The floor diaphragm has 3-layer CLT panels and the SC-CLT wall has 5-layer CLT panels. Two glulam collector beams are connected to the SC-CLT wall, one on each side of the wall. The collector beams transfer the in-plane (i.e., north–south, in the direction of the SC-CLT wall) lateral forces from the CLT floor diaphragm to the SC-CLT wall. The gravity load system consists of glulam gravity beams and gravity columns with pinned bases. The glulam material was provided by Western Structures (Eugene, Oregon) and fabricated from Douglas fir (DF) lumber.

The SC-CLT wall, shown in Fig. 4, has two post-tensioned wall panels (i.e., the north panel and south panel, denoted NWP and SWP, respectively). Each panel is approximately 175 mm thick (t_w), 1,524 mm long (L_w), and 6.1 m tall (H_w). The moisture content of the CLT wall panels was measured at the time of the subassembly tests and found to be approximately 6.5% and 8.8% for the UT specimen and MT specimen, respectively. The CLT wall panels rest on a concrete foundation, cast on a steel beam attached to the lab strong floor, simulating a stiff building foundation. The concrete foundation surface enables relatively uniform bearing stresses along the base of the wall panels. Each CLT wall panel was post-tensioned with a 32-mm-diameter PT steel bar that is

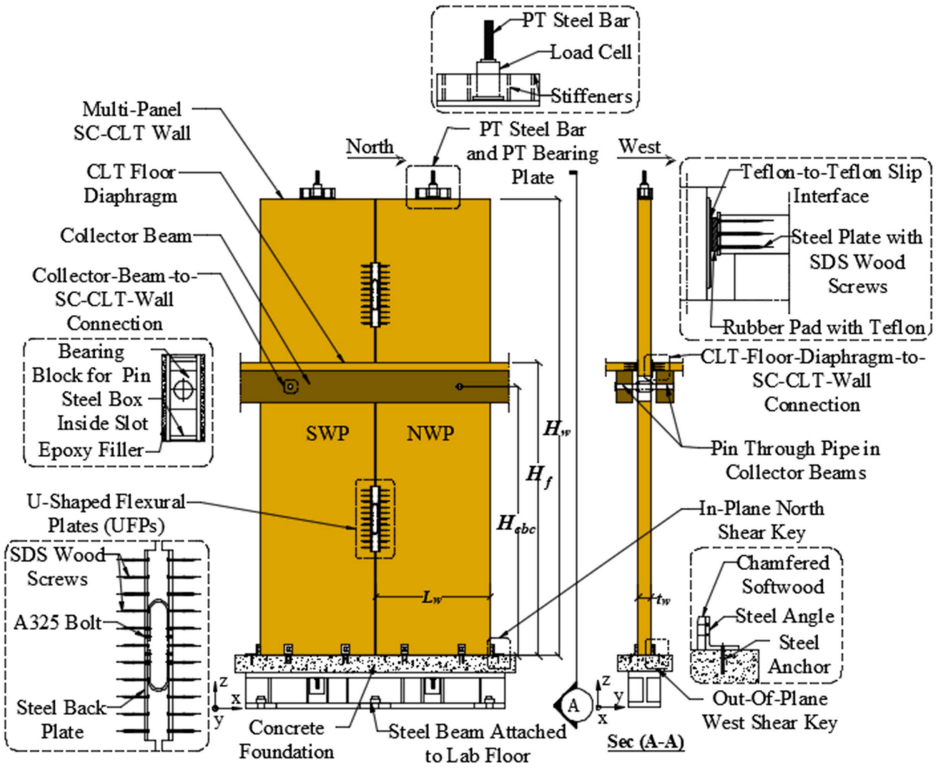

Fig. 4. Test subassembly multipanel SC-CLT wall details.

anchored to the foundation. The inner ply at the midlength of each CLT wall panel was removed by the manufacturer to allow the PT steel bar to pass through the center of the CLT wall panel. The prestressing ratios f_{pi}/f_{pu}, where f_{pi} is the initial prestress and f_{pu} is the ultimate stress of the PT steel bar, are approximately 0.35 and 0.40 for the UT and MT specimens, respectively. This slight difference was unintended and due to imprecision in the post-tensioning operations for the two test specimens. The f_{py} is the PT steel bar stress at yielding and is equal to 834 MPa (i.e., $0.81f_{pu}$). A stiffened steel PT bearing plate (Fig. 4) supports the PT bar anchorage at the top of each CLT wall panel and distributes the PT bar force into the wall panel without excessive bearing deformation of the CLT material. During the short time between the post-tensioning operation and the beginning of each cyclic lateral loading test, no significant loss in PT bar forces was observed. Shear keys (Fig. 4), at the north and south edges of the SC-CLT wall (i.e., in-plane shear keys) and at the east and west faces of each CLT wall panel (i.e., out-of-plane shear keys), are attached to the concrete foundation to prevent sliding of the wall and transfer the base shear to the foundation. Each shear key consists of chamfered softwood placed between the CLT wall panel and a steel angle anchored to the foundation. The chamfered softwood prevented the steel angle from causing local damage to the CLT wall panels. A shear key was placed in between the CLT wall panels in the MT specimen to improve the test setup and avoid early end rolling damage of the CLT wall panels due to sliding.

The collector-beam-to-SC-CLT-wall connection (Fig. 4) in the test subassembly consists of a round steel pin placed through a steel block in a vertical slot in each wall panel (Amer 2023). The vertical slot enables each CLT wall panel to rock without causing uplift of the collector beams. The height of the collector-beam-to-SC-CLT-wall connection from the top of the foundation H_{cbc} is 3.6 m. Rubber bearings (Fig. 4) with a sliding Teflon-to-Teflon slip interface transfer out-of-plane loading from the floor diaphragm to the SC-CLT wall, and provide out-of-plane bracing to the SC-CLT wall without damage to the CLT floor panels. The adjacent CLT wall panels are connected with pairs of UFPs, shown in Fig. 4 (one UFP was omitted above the floor diaphragm in the MT specimen), that are recessed in the wall and anchored to it using Simpson Strong-Tie (Denver) SDS wood screws for energy dissipation. Hence, four UFPs are used in the UT specimen and three UFPs are used in the MT specimen, with two UFPs below and one UFP above the CLT floor diaphragm. The UFP strength was selected to provide an energy dissipation ratio (Seo and Sause 2005) of less than 50%. More details of the test subassembly can be found in Amer (2023).

Test Setup and Loading Control Scheme

In the test setup, two in-plane actuators (Fig. 3), one below and one above the floor diaphragm, load a transverse beam connected to the floor diaphragm to displace the test subassembly in the in-plane (i.e., north–south) direction. Two out-of-plane actuators (Fig. 3) are connected to the floor diaphragm to displace the test subassembly in the out-of-plane (i.e., east–west) direction. The multidirectional displacements of the test subassembly are specified and controlled at the so-called structure-physical-node (SPN) (Fig. 3). The SPN is at a point in space at the top of the floor diaphragm and in the middle of the SC-CLT wall. The top of the floor diaphragm above the foundation H_f is approximately 3.92 m. Multidirectional displacements are imposed on the test subassembly to reach a predefined target floor diaphragm story drift, denoted Θ_d^{target}, which is the target horizontal displacement of the SPN divided by H_f, and is given in percent (%) radians. The in-plane and out-of-plane target floor diaphragm story drifts are denoted $\Theta_{d,x}^{\text{target}}$ and $\Theta_{d,y}^{\text{target}}$, respectively. Continuous feedback from displacement sensors attached to the floor diaphragm provides the displaced position of the SPN (Mercan et al. 2009; Sause et al. 2020; Amer 2023).

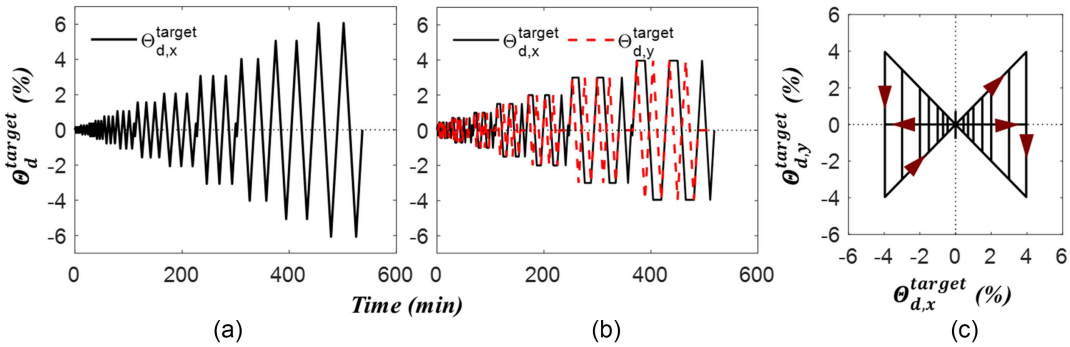

Fig. 5. Quasi-static cyclic loading protocol (note that stops for inspection are not shown): (a) UT history of imposed in-plane floor diaphragm story drift, $\Theta_{d,x}^{\text{target}}$; (b) MT history of imposed in-plane and out-of-plane floor diaphragm story drifts, $\Theta_{d,x}^{\text{target}}$ and $\Theta_{d,y}^{\text{target}}$, respectively; and (c) associated multidirectional bow-tie-shaped loading path used in MT.

Loading Protocol

The test subassembly was subjected to quasi-static cyclic loading consistent with the American Concrete Institute (ACI 2007) testing protocol. Positive story drifts correspond to displacements in north and west directions (Fig. 3). The peak value of Θ_d^{target} is denoted $\hat{\Theta}_d^{\text{target}}$, and peak values of $\Theta_{d,x}^{\text{target}}$ and $\Theta_{d,y}^{\text{target}}$ are denoted $\hat{\Theta}_{d,x}^{\text{target}}$ and $\hat{\Theta}_{d,y}^{\text{target}}$, respectively. In the UT, the test subassembly was subjected to monotonically increasing quasi-static cyclic in-plane loading shown in Fig. 5(a) with three cycles of drift applied up to $\hat{\Theta}_{d,x}^{\text{target}} = 3.0\%$ and two cycles of drift applied up to $\hat{\Theta}_{d,x}^{\text{target}} = 6.0\%$. In the MT, the test subassembly was subjected to a multidirectional loading protocol shown in Fig. 5(b), which follows the bow-tie-shaped loading path shown in Fig. 5(c) up to $\hat{\Theta}_d^{\text{target}} = 4.0\%$. The test subassembly was not subjected to torsional motion (in the plane of the CLT floor diaphragm).

Instrumentation

The measured horizontal displacement of the SC-CLT wall is obtained by averaging the displacements of the two CLT wall panels, each measured by string potentiometers attached at the top of the CLT wall panel above the floor diaphragm elevation (Amer 2023). Linear potentiometers (LPs) (Fig. 6) on each CLT panel were used to measure the vertical motion (e.g., gap opening) and panel contact with the foundation along the panel base. Data from the LPs were transformed to the face of the CLT wall panel to account for the eccentricity, e, shown in Fig. 6, from the mounting fixtures. The force in each PT steel bar was measured by a load cell (Fig. 4). Each gravity column has an instrumented pin to measure the in-plane shear force in the column. Each actuator has a load cell to measure the force applied to the test subassembly. The SC-CLT wall in-plane base shear is calculated by subtracting the measured in-plane shear forces of the gravity columns from the in-plane component of the applied forces measured by the actuator load cells. The test subassembly out-of-plane base shear was the out-of-plane component of the applied forces measured by the actuator load cells.

SC-CLT Wall Experimental Results

SC-CLT Wall Damage States

As an SC-CLT wall rocks on the foundation, the CLT panel corners are subjected to compression [Fig. 1(a)], so the compression stress–strain behavior of the CLT wall panel material in the UT specimen was determined by tests on five compression specimens (CSs) taken from an untested CLT panel (Amer 2023). In the CS tests, damage was observed to concentrate within a length equal to t_w, so the height of the compression failure zone in the SC-CLT wall panels H_{cr} is assumed equal to t_w (Kurama et al. 1999a, b; Perez et al. 2007; Akbas et al. 2017; Amer 2023). The compression stress–strain behavior of the CLT material from the CS test results is shown in Fig. 7.

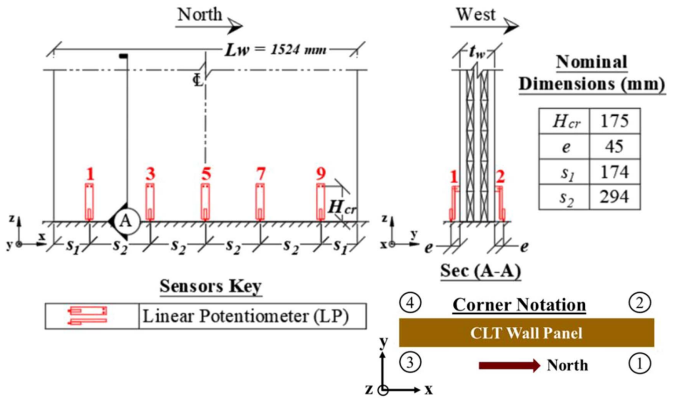

Fig. 6. Instrumentation layout: elevation view and cross-sectional view of CLT wall panel base and CLT wall panel corner notation.

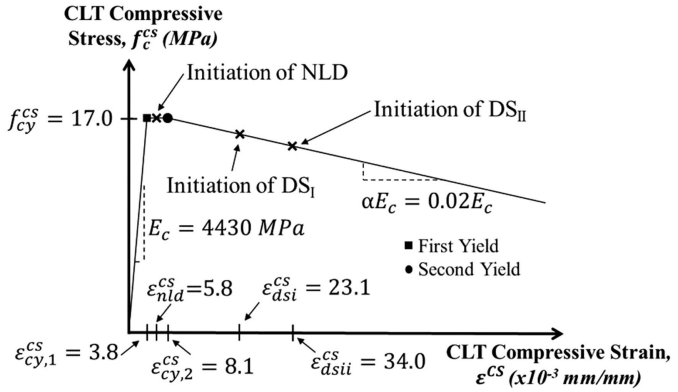

Fig. 7. Compression stress–strain behavior and damage states of CLT material from CS tests.

Table 2. Test results for first occurrence of damage at wall corner

Test	Damage state	Identifier	CLT wall panel corner	Floor diaphragm story drift		SC-CLT wall story drift		CLT compression strain	Cycle no.
				$\hat{\Theta}_{d,x}$ (%)	$\hat{\Theta}_{d,y}$ (%)	$\hat{\Theta}_{w,x}$ (%)	$\hat{\Theta}_{w,y}$ (%)	$\hat{\varepsilon}_e$ ($\times 10^{-3}$ mm/mm)	
UT	NLD	NLD-b	NWP-2	0.51	0.00	0.41	−0.08	6.8	3
UT	DS_I	DS_I-a, c	NWP-1	1.56	0.00	1.53	−0.09	14.7	1
UT	DS_{II}	DS_{II}-b	SWP-1	3.07	0.00	3.13	−0.09	31.8	1
MT	NLD	NLD-a	SWP-2	0.28	0.00	0.24	0.00	16.0	1
MT	DS_I	DS_I-a	NWP-2	0.44	0.45	0.41	0.48	22.8	1
MT	DS_{II}	DS_{II}-c	SWP-1	2.0	−2.0	2.04	−2.10	32.3	1

The SC-CLT wall damage states, summarized in Table 1, were quantified in terms of EDPs, which are representative of the lateral-load response of the SC-CLT wall and the test subassembly. The SC-CLT wall corners were inspected after each half-cycle of the lateral displacement history imposed to the test subassembly (i.e., the test subassembly returned to zero). The observed damage is associated with an EDP value measured at the maximum amplitude of story drift of the completed half-cycle (Amer et al. 2022). For each damage state, three EDP values and the cycle number associated with the first visible damage (Table 1) are documented for all eight corners of the SC-CLT wall [full data sets are available in Amer (2023)]. For each damage state, the first observed damage form varied among the corners of the SC-CLT wall and the initiation of the damage was observed to concentrate within H_{cr} (i.e., similar to the CS test results). The three EDP values are (1) the measured peak floor diaphragm story drift, Θ_d; (2) the simultaneous SC-CLT wall story drift, Θ_w; and (3) the simultaneous CLT wall panel corner compression strain, ε_e. Story drift Θ_d is the measured position of the SPN divided by H_f and is given in percent (%) radians. The in-plane and out-of-plane values of Θ_d are denoted $\Theta_{d,x}$ and $\Theta_{d,y}$, respectively. The in-plane and out-of-plane values of Θ_w are denoted $\Theta_{w,x}$ and $\Theta_{w,y}$, respectively. The Θ_d and Θ_w were not identical due to modest levels of deformation in the connections between the wall and the diaphragm in the test subassembly. ε_e is the measured axial deformation (i.e., over the length H_{cr}) of the CLT wall panel compression corner divided by H_{cr}. This axial deformation is from linear extrapolation of measurements from the LPs to the wall corners, where as shown in Fig. 6, the LPs have equal gauge lengths of H_{cr}. Note that ε_e is not a local strain; rather, ε_e is the average compression strain over the height of the failure zone, H_{cr}. The CLT wall panel corner notation (e.g., the northeast corner of the NWP is denoted NWP-1) is shown in Fig. 6.

Table 2 lists the measured peak in-plane floor diaphragm story drift when a damage state was *first* observed at any of the eight corners of the wall, $\hat{\Theta}_{d,x}$, the simultaneous out-of-plane floor diaphragm story drift, $\hat{\Theta}_{d,y}$, the simultaneous in-plane and out-of-plane SC-CLT wall story drift, $\hat{\Theta}_{w,x}$ and $\hat{\Theta}_{w,y}$, and the simultaneous CLT wall panel corner compression strain, $\hat{\varepsilon}_e$. The table shows that the values for $\hat{\Theta}_{d,x}$ when a damage state was first observed are smaller for the MT than for the UT. NLD, DS_I, and DS_{II} were first observed under unidirectional loading (in the UT) at $\hat{\Theta}_{w,x} =$ 0.41%, 1.53%, and 3.13%, respectively, and under multidirectional loading (in the MT) at $\hat{\Theta}_{w,x} = 0.24\%$, 0.41%, and 2.04%, respectively. This result is expected, because the CLT wall panel is under nearly uniform compression strain through the thickness of the panel under unidirectional loading, but the compression strain is concentrated in the outer ply of the panel under multidirectional loading. At NLD, the value of $\hat{\varepsilon}_e$ from the UT is close to the value of ε_{nld}^{cs} and $\varepsilon_{cy,2}^{cs}$ (Fig. 7), while the difference between the value of $\hat{\varepsilon}_e$ from the MT and ε_{nld}^{cs} and $\varepsilon_{cy,2}^{cs}$ is large. At DS_I, the value of $\hat{\varepsilon}_e$ from the MT is close to the value of ε_{dsi}^{cs} and the difference between the value of $\hat{\varepsilon}_e$ from the UT and ε_{dsi}^{cs} is large. At DS_{II}, however, the difference between the values of $\hat{\varepsilon}_e$ from the UT and MT and ε_{dsii}^{cs} is less than 10%. Fig. 8(a) shows the lateral-load response of the SC-CLT wall, based on $\hat{\Theta}_{w,x}$, and points when damage was first observed for loading cycles up to $\hat{\Theta}_d^{\text{target}} = 3.0\%$.

The DS_{III} damage state was not reached in the UT or MT. In the UT, the test subassembly was loaded up to $\hat{\Theta}_{d,x}^{\text{target}} = 6.0\%$, and a decrease in $V_{w,x}$ of only 8.0% was observed in the second cycle to $\hat{\Theta}_{d,x}^{\text{target}} = 6.0\%$. Fig. 8(b) shows a detail of the in-plane lateral-load response of the SC-CLT wall from the MT at $\hat{\Theta}_{d,x}^{\text{target}} = 4.0\%$. A decrease in $V_{w,x}$ was observed under multidirectional loading, for each bow-tie shaped cycle at the same $\Theta_{w,x}$, due to test subassembly relaxation when the out-of-plane loading is reversed from west to east [i.e., from Point a to Point b in Fig. 8(b)] and the observed damage of the CLT wall panels. A decrease of 13.4% in $V_{w,x}$ was observed in the first cycle [i.e., between Points 1-a and 1-b in Fig. 8(b)] and a decrease of 14.4% in $V_{w,x}$ was observed in the second cycle [i.e., between Points 2-a and 2-b in Fig. 8(b)] with $\hat{\Theta}_{d,x}^{\text{target}} = 4.0\%$. Compared to the peak $V_{w,x}$ for the first cycle [Point 1-a in Fig. 8(b)], a decrease of 6.0% in $V_{w,x}$ was observed in the second cycle (i.e., between Points 1-a and 2-a) and a decrease of 10.9% in $V_{w,x}$ was observed in the third cycle (i.e., between Points 1-a and 3-c) with $\hat{\Theta}_{d,x}^{\text{target}} = 4.0\%$.

Estimates of SC-CLT Wall Limit States and Damage States

This section compares the measured SC-CLT wall limit states and damage states results from the UT with estimates from closed-form expressions (CFEs) presented in Akbas (2016) and Akbas et al. (2017). The development of the CFE (Akbas 2016) assumes that the SC-CLT wall is under in-plane loading only. The comparison is based on equivalence of the compression strain used in the CFE with the measured CLT wall panel corner compression strain from the UT. In applying the CFE, the compression stress–strain behavior of the CLT material is based on the CS test results shown in Fig. 7.

The DEC and ELL limit states are not based on local compression strain and only the YCLT limit state is considered in the comparison (Amer 2023). Two YCLT limit states are considered; YCLT Limit State 1 is the first CLT material yield point where the strain is $\varepsilon_{cy,1}^{cs}$, and YCLT Limit State 2 is the second yield point where the strain is $\varepsilon_{cy,2}^{cs}$ (Fig. 7). Table 3 compares estimated results from the CFE with measured UT results at the YCLT limit state. In Table 3, $\overline{\varepsilon_e}$ is the average measured strain of the compression corners of the

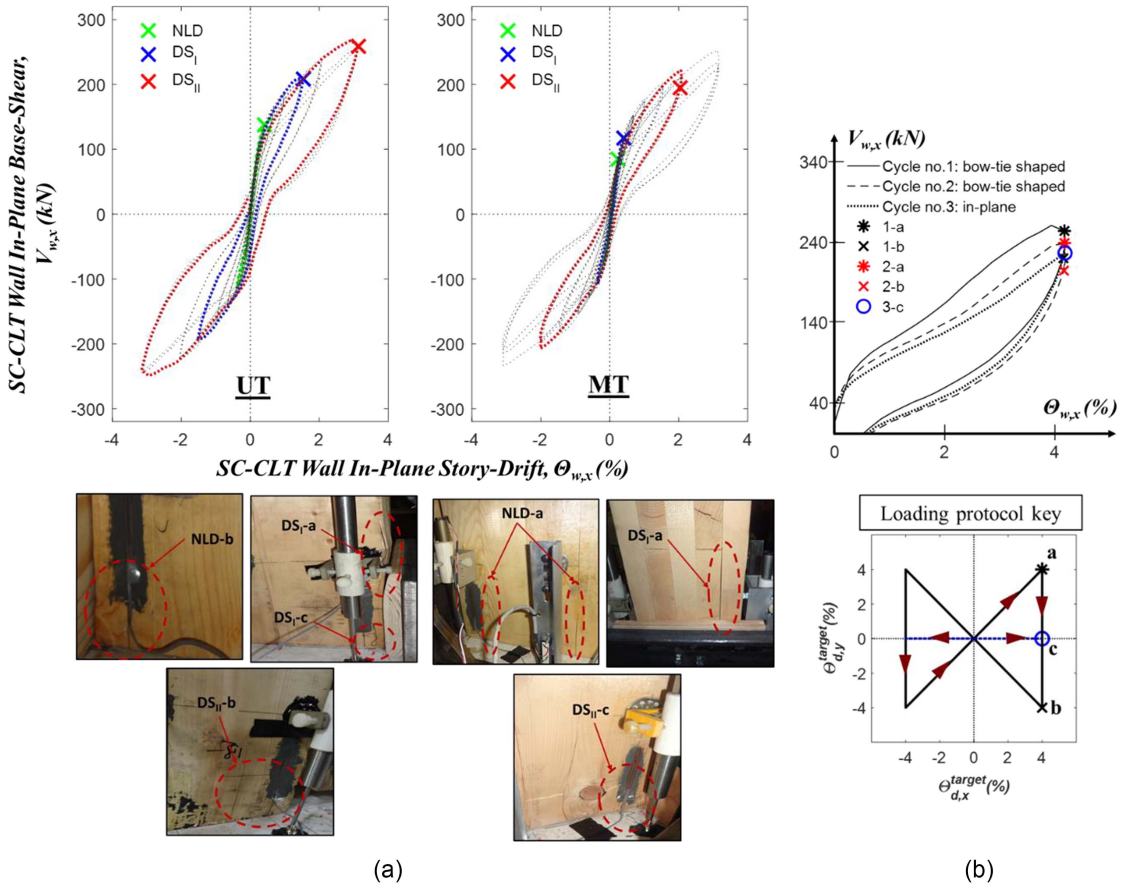

Fig. 8. (a) Comparison of in-plane lateral-load response, initiation of SC-CLT wall damage states, and associated photographs of damage from UT and MT up to $\hat{\Theta}_d^{\text{target}} = 3.0\%$; and (b) close-up view of in-plane cyclic lateral-load response of SC-CLT wall at $\hat{\Theta}_d^{\text{target}} = 4.0\%$ in MT.

Table 3. Comparison of CFE results and UT results at YCLT limit state

Loading direction	CLT wall panel	i	$\overline{\varepsilon_e} = \varepsilon_{cy,i}^{cs}$ ($\times 10^{-3}$ mm/mm)	CFE			UT		
				θ_{el}^{ce} (%)	θ_b^{cfe} (%)	$\theta_{wp,x}^{cfe}$ (%)	θ_{el} (%)	θ_b (%)	$\theta_{wp,x}$ (%)
North	NWP	1	3.8	0.22	0.23	0.45	0.15	0.12	0.27
South	SWP	1	3.8	0.22	0.23	0.45	0.22	0.21	0.43
North	NWP	2	8.1	0.26	0.66	0.92	0.33	0.35	0.68
South	SWP	2	8.1	0.26	0.66	0.92	0.33	0.65	0.98

NWP (i.e., NWP-1 and NWP-2) for loading in the north direction, and the average measured strain of the compression corners of the SWP (i.e., SWP-3 and SWP-4) for loading in the south direction. The θ_b values given in Table 3 are the measured CLT wall panel base rotations obtained from a linear fit to the LP data from the CLT wall panel base (Fig. 6) and the $\theta_{wp,x}$ values are the simultaneous measured CLT wall panel in-plane story drifts, when $\overline{\varepsilon_e}$ is equal to $\varepsilon_{cy,1}^{cs}$ or $\varepsilon_{cy,2}^{cs}$. The value of θ_{el} is obtained by subtracting θ_b from $\theta_{wp,x}$. The results from the CFE, with the superscript cfe, are calculated assuming the compression strain in the CFE equals $\varepsilon_{cy,1}^{cs}$ or $\varepsilon_{cy,2}^{cs}$. Better agreement between θ_b^{cfe} and θ_b is observed for the SWP compared to the NWP. Differences between θ_b^{cfe} and θ_b are expected to be small because the compression strain used in the CFE is equal to $\overline{\varepsilon_e}$ in the UT. Discrepancies in the results between θ_{el}^{cfe} and θ_{el} for the NWP and SWP are observed because the elastic material properties used in the CFE, derived from the CS tests, may not accurately represent the elastic tensile or shear stress–strain behavior of the CLT material. Better agreement between the CFE and UT results is observed for the SWP. No damage to the corners of the CLT wall panels was observed in the UT when $\overline{\varepsilon_e}$ was equal to $\varepsilon_{cy,1}^{cs}$.

Table 4 shows predictions of SC-CLT wall damage states using the CFE with strain values equal to the strains for observed damage in the CS tests (Fig. 7). The predictions are compared with UT results for the *first* occurrence of damage at corner NWP-1 or NWP-2 for loading in the north direction and corner SWP-3 or SWP-4 for loading in the south direction. The strain values for the UT are the average measured strain of the compression corners (of the NWP or SWP) simultaneous to $\hat{\Theta}_{d,x}$ corresponding to the first observed damage. The CFE predictions of θ_b for the first occurrence of damage are reasonable relative to the UT results (considering the variability in the test data, discussed previously); however, the values of θ_{el} from the CFE are generally less than the UT results.

J. Struct. Eng., 2024, 150(2): 04023215

Table 4. Comparisons of SC-CLT wall damage state predictions using CS strains and UT results for first occurrence of damage at wall corner

Damage state	Loading direction	CLT wall panel	CFE				UT			
			ε^{CS} ($\times 10^{-3}$ mm/mm)	θ_{el}^{cfe} (%)	θ_{b}^{cfe} (%)	$\theta_{wp,x}^{cfe}$ (%)	$\overline{\varepsilon_e}$ ($\times 10^{-3}$ mm/mm)	θ_{el} (%)	θ_{b} (%)	$\theta_{wp,x}$ (%)
NLD	North	NWP	5.8	0.24	0.44	0.68	5.9	0.23	0.21	0.44
NLD	South	SWP	5.8	0.24	0.44	0.68	5.8	0.14	0.54	0.68
DS_I	North	NWP	23.1	0.31	1.75	2.06	17.2	0.57	1.03	1.60
DS_I	South	SWP	23.1	0.31	1.75	2.06	21.1	0.41	1.65	2.06
DS_{II}	North	NWP	34.0	0.33	2.34	2.67	35.5	0.85	2.39	3.24
DS_{II}	South	SWP	34.0	0.33	2.34	2.67	38.2	0.40	2.77	3.17

Effects of SC-CLT Wall Damage on SC-CLT Wall Lateral-Load Response

To show the effects of SC-CLT wall damage on the lateral-load response, values of $V_{w,x}$ at the third cycle of loading to a given $\hat{\Theta}_d^{\text{target}}$ after a damage state is reached were used to quantify the effects of the damage. Following the initiation of the NLD damage state, and subsequent initiation of DS_I, no decrease in $V_{w,x}$ was observed in either test. In the UT, $V_{w,x}$ decreased by 6.8% and 4.1% after the initiation of DS_{II} for loading in the north and south directions, respectively. In the MT, $V_{w,x}$ decreased by 4.4% and 10.6% after the initiation of DS_{II} for loading in the north and south directions, respectively. These results suggest that a repair action is needed after DS_{II} is reached to restore the lateral-load response of the SC-CLT wall.

The decrease in the PT bar force during subsequent loading cycles following the initiation of NLD and DS_I is insignificant. After the initiation of DS_{II}, the decrease in the NWP and SWP PT bar force is 6.6% and 7.1%, respectively, for the UT, and 4.2% and 3.4%, respectively, for the MT, which are considered relatively insignificant. The PT steel bars did not yield in either test.

Fragility Functions for SC-CLT Wall Damage States

Fragility functions for damage states of an individual SC-CLT wall panel corner in compression (i.e., a component) or an entire SC-CLT wall (i.e., a system) were developed from the experimental results. The fragility functions provide the probability of reaching or exceeding a selected damage state, ds_i, conditioned on a given EDP. For each damage state (Table 1), the EDP values when the damage was *first* observed at *each* of the eight corners of the SC-CLT wall are given in Amer (2023). These EDP values are quite variable for both the UT and MT, reflecting the uncertainty in the damage state criteria and test observations, and the variability in CLT material properties.

Component-Level Fragility Functions

The variability in the EDP value when a damage state was first observed for each of the eight corners of the SC-CLT wall specimens was used to quantify the uncertainty in wall panel corner (i.e., component) damage occurrence. For each damage state and each EDP, two sets of sample data points (i.e., the EDP values for damage state, ds_i) for the first observed damage at each wall panel corner are available; one set from the UT and one set from the MT. A lognormal distribution is assumed to fit each set of sample data, and the lognormal mean and standard deviation of the sample data, denoted λ_o and ζ_o, respectively, are estimated using maximum likelihood estimators (Ang and Tang 2007). The geometric mean of the sample data $\bar{\lambda}_o$ is equal to the exponential of λ_o and corresponds to 50% probability of reaching or exceeding the selected damage state.

Given the small size of each sample data set (i.e., eight data points for each damage state and each EDP from the UT or MT), the procedure recommended by Chiozzi and Miranda (2017) is followed to test the fit of the lognormal distribution to the data sets. Tables 5 and 6 summarize the estimated parameters of the lognormal distribution fit to the sample data sets. The $\bar{\lambda}_o$ values for $\Theta_{d,x}$ and $\Theta_{w,x}$ as the EDP are approximately 28%, 44%, and 13% smaller for the MT (i.e., multidirectional loading) compared to the UT (i.e., unidirectional loading) for NLD, DS_I, and DS_{II}, respectively. The $\bar{\lambda}_o$ values for ε_e as the EDP are the same for the MT and UT for DS_I, but are 76% and 10% larger for the MT compared to the UT for NLD and DS_{II}, respectively. For NLD, the $\bar{\lambda}_o$ values for ε_e for both the UT and MT are significantly larger than

Table 5. Estimated lognormal distribution parameters from sample data for component damage states with $\Theta_{d,x}$ and $\Theta_{w,x}$ as EDPs

Test	EDP	NLD			DS_I			DS_{II}		
		$\bar{\lambda}_o$ (%)	λ_o	ζ_o	$\bar{\lambda}_o$ (%)	λ_o	ζ_o	$\bar{\lambda}_o$ (%)	λ_o	ζ_o
UT	$\Theta_{d,x}$	1.01	0.010	0.612	2.27	0.819	0.373	3.39	1.221	0.140
UT	$\Theta_{w,x}$	0.91	−0.091	0.684	2.28	0.824	0.396	3.49	1.251	0.145
MT	$\Theta_{d,x}$	0.73	−0.310	0.729	1.29	0.252	0.252	2.95	1.082	0.184
MT	$\Theta_{w,x}$	0.67	−0.393	0.787	1.27	0.239	0.238	3.05	1.115	0.193

Table 6. Estimated lognormal distribution parameters from sample data for component damage states with ε_e as EDP

Test	NLD			DS_I			DS_{II}		
	$\bar{\lambda}_o$ ($\times 10^{-3}$ mm/mm)	λ_o	ζ_o	$\bar{\lambda}_o$ ($\times 10^{-3}$ mm/mm)	λ_o	ζ_o	$\bar{\lambda}_o$ ($\times 10^{-3}$ mm/mm)	λ_o	ζ_o
UT	10.7	2.365	0.733	25.7	3.247	0.466	42.3	3.746	0.214
MT	18.8	2.936	0.394	25.8	3.250	0.445	46.5	3.840	0.204

Table 7. Estimated population lognormal distribution parameters for component damage states with $\Theta_{d,x}$ and $\Theta_{w,x}$ as EDPs

		NLD			DS_I			DS_{II}		
Loading	EDP	$\bar{\lambda}$ (%)	λ	ζ	$\bar{\lambda}$ (%)	λ	ζ	$\bar{\lambda}$ (%)	λ	ζ
U	$\Theta_{d,x}$	1.01	0.010	0.490	2.27	0.819	0.320	3.39	1.221	0.179
U	$\Theta_{w,x}$	0.91	−0.091	0.542	2.28	0.824	0.335	3.49	1.251	0.182
M	$\Theta_{d,x}$	0.73	−0.310	0.575	1.29	0.252	0.559	2.95	1.082	0.201
M	$\Theta_{w,x}$	0.67	−0.393	0.618	1.27	0.238	0.589	3.05	1.115	0.206

Note: U = unidirectional loading; and M = multidirectional loading.

Table 8. Estimated population lognormal distribution parameters for component damage states with ε_e as EDP

	NLD			DS_I			DS_{II}		
Loading	$\bar{\lambda}$ ($\times 10^{-3}$ mm/mm)	λ	ζ	$\bar{\lambda}$ ($\times 10^{-3}$ mm/mm)	λ	ζ	$\bar{\lambda}$ ($\times 10^{-3}$ mm/mm)	λ	ζ
U	10.7	2.365	0.578	25.7	3.247	0.384	42.3	3.746	0.218
M	18.8	2.936	0.334	25.8	3.250	0.376	46.5	3.840	0.212

Note: U = unidirectional loading; and M = multidirectional loading.

ε_{nld}^{cs} (Fig. 7), which is the average value from the CLT material CS tests. For DS_I, the $\bar{\lambda}_o$ values for ε_e are approximately 12% larger than ε_{dsi}^{cs} (i.e., the average value from the CS tests) for both the UT and MT. For DS_{II}, the $\bar{\lambda}_o$ value for ε_e is 24.4% and 36.8% larger than ε_{dsii}^{cs} for the UT and MT, respectively. The $\bar{\lambda}_o$ values for ε_e, for a given damage state, are anticipated to be larger than the strains from the CS tests because the largest compression strain is localized at a CLT wall panel corner in the lateral-load tests while the entire cross-section area of the CS is under uniform compression strain. The ζ_o is a measure of the sample data dispersion and is different for each damage state and each EDP for both the UT and MT. The value of ζ_o ranges from 0.14 to 0.79, and this wide range is likely from the small size of the sample data sets and using EDP values corresponding to the peak floor diaphragm story drift within a loading cycle to quantify the damage states.

The unexpectedly wide range of ζ_o values suggests using a Bayesian approach to estimate the population lognormal standard deviation, ζ, for each damage state and each EDP. The lognormal mean of the population, λ, is assumed to be equal to the lognormal mean of the sample data, λ_o. Bayesian updating was applied to the lognormal variance (of the population), denoted β, which equals ζ^2 and is treated as a random variable. An inverse gamma distribution with shape parameter a and scale parameter b was used as the conjugate prior distribution for β (Lynch 2007). The posterior distribution, which is the updated distribution after observing the sample data, is proportional to the product of the prior distribution and likelihood function (Lynch 2007). The posterior distribution has an inverse gamma distribution with parameters $a_{\text{post}} = a + n/2$ and b_{post}, determined from Eq. (1), where x_i is the ith value of the EDP in the sample data for a selected ds_i and n is the size of the sample data set. The mean of the posterior distribution, $\mu_{\beta,\text{post}} = b_{\text{post}}/(a_{\text{post}} - 1)$, is the expected value of the lognormal variance β (for the population)

$$b_{\text{post}} = b + \frac{1}{2}\sum_{i=1}^{n}[\ln(x_i) - \lambda]^2 \tag{1}$$

The values of the parameters a and b of the prior distribution for β were selected so the mean of the prior distribution, $\mu_{\beta,\text{prior}} = b/(a-1)$, is equal to 0.0625, which corresponds to an assumed prior lognormal standard deviation of 0.25 and is considered to be appropriate for timber material properties (Ross 2010). Also, the values of a and b were selected such that the lognormal variance of the sample data, which is equal to ζ_o^2, falls in the range of $\mu_{\beta,\text{post}} \pm 2\sigma_{\beta,\text{post}}$ (i.e., based on selecting 95% confidence interval), where $\sigma_{\beta,\text{post}}$ is the standard deviation of the posterior distribution. Tables 7 and 8 summarize the population lognormal mean and standard deviation for the component damage states, λ and ζ, respectively, from the Bayesian updating. The value of λ is assumed to be equal to λ_o and ζ is equal to $\sqrt{\mu_{\beta,\text{post}}}$. Note that ζ ranges from 0.18 to 0.62, which is about 2/3 of the range of ζ_o.

The probability of a component reaching or exceeding a selected damage state ds_i conditioned on an EDP, denoted $P(F_{\text{comp}}|\text{EDP} = x)$, is as follows:

$$P(F_{\text{comp}}|\text{EDP} = x) = P(\text{DS} \geq ds_i|\text{EDP} = x) = \Phi\left(\frac{\ln(x) - \lambda}{\zeta}\right) \tag{2}$$

where Φ is the standard normal cumulative distribution function. Figs. 9(a and b) show the component fragility functions conditioned on $\Theta_{d,x}$ and $\Theta_{w,x}$, respectively, for unidirectional and multidirectional loading. The figures show that for a given EDP value, the probability of a component (i.e., wall panel corner) reaching or exceeding a given ds_i is larger for multidirectional loading compared to unidirectional loading, consistent with previous observations that multidirectional loading causes damage at smaller story-drift levels than unidirectional loading.

Fig. 9(c) shows the component fragility functions with ε_e as the EDP for unidirectional and multidirectional loading. For the same probability of a component reaching or exceeding DS_I, ε_e for unidirectional loading and multidirectional loading are similar, while for the same probability of a component reaching or exceeding NLD or DS_{II}, ε_e for multidirectional loading is larger than for unidirectional loading. As previously mentioned, a CLT wall panel is under approximately uniform compression strain through the thickness of the CLT wall panel under unidirectional loading, while the compression strain is concentrated in an outer ply of the CLT panel under multidirectional loading and the adjacent ply with smaller compression strain provides some support to the outer ply with larger concentrated strain. Hence, for the same compression strain, the probability of a wall corner reaching or exceeding a given damage state is smaller when the wall is subjected to multidirectional loading compared to unidirectional loading. When using this

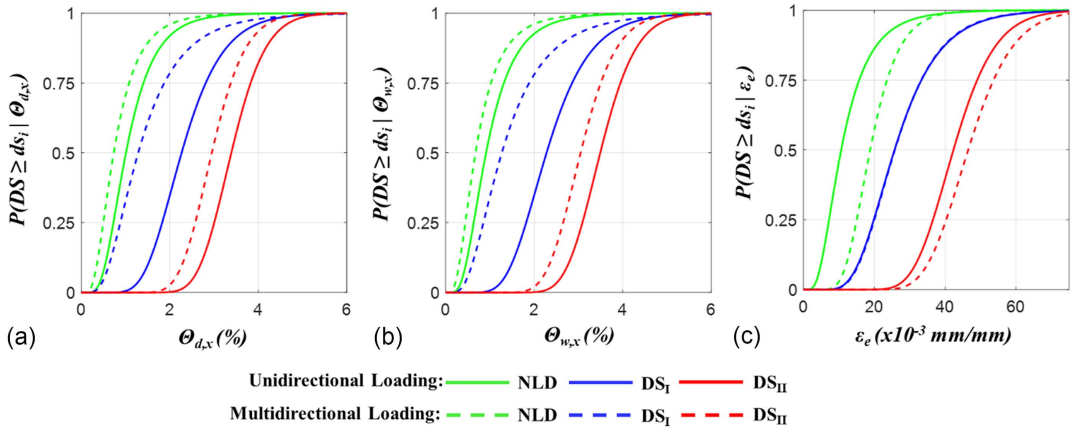

Fig. 9. Component fragility with EDP as (a) $\Theta_{d,x}$; (b) $\Theta_{w,x}$; and (c) ε_e.

Table 9. Estimated lognormal distribution parameters for approximate upper-bound fragilities for system damage states

		NLD			DS_I			DS_{II}		
Loading	EDP	$\bar{\lambda}_{sys}$ (%)	λ_{sys}	ζ_{sys}	$\bar{\lambda}_{sys}$ (%)	λ_{sys}	ζ_{sys}	$\bar{\lambda}_{sys}$ (%)	λ_{sys}	ζ_{sys}
U	$\Theta_{d,x}$	0.51	−0.668	0.275	1.46	0.376	0.180	2.64	0.972	0.101
U	$\Theta_{w,x}$	0.43	−0.841	0.305	1.43	0.360	0.189	2.71	0.999	0.102
M	$\Theta_{d,x}$	0.33	−1.105	0.323	0.59	−0.523	0.315	2.23	0.803	0.113
M	$\Theta_{w,x}$	0.29	−1.250	0.350	0.56	−0.578	0.332	2.29	0.829	0.116

Note: U = unidirectional loading; and M = multidirectional loading.

information in a numerical simulation to predict damage probabilities under multidirectional loading, the simulation must accurately estimate the corner compression strain from simultaneous in-plane and out-of-plane loading.

System-Level Fragility Functions

To represent the probability of an entire SC-CLT wall, rather than an individual CLT wall panel corner, being in a selected damage state, the SC-CLT wall can be considered as a system composed of a number of components. The components are treated as series components, because damage to one wall corner is considered to be damage to the entire wall. The SC-CLT walls studied here, with two CLT wall panels, are treated as systems with eight components (i.e., the eight CLT wall panel corners) in series. The SC-CLT wall damage state ds_i is reached if one or more of these components reaches the given ds_i. All wall corners (i.e., all components) are assumed to have the same fragility for each ds_i and each EDP. The system fragility function provides the probability of the system reaching or exceeding a given ds_i, conditioned on a given EDP, and is denoted $P(F_{\text{sys}}|\text{EDP} = x)$. Using first-order reliability theory, the lower and upper bounds on $P(F_{sys}|\text{EDP} = x)$ are as follows. The lower bound (LB) represents the case where the component failure (i.e., damage) events are fully correlated, and the system fragility equals the component fragility [i.e., $P(F_{sys}|\text{EDP} = x) = P(F_{comp}|\text{EDP} = x)$]. The upper bound (UB) represents the case where the component failure (i.e., damage) events are fully independent (i.e., $P(F_{sys}|\text{EDP} = x) = 1 - \prod_{i=1}^{m}[1 - P(F_{comp}|\text{EDP} = x)]$, where m is the number of the components in the system).

To more conveniently quantify the UB system fragility, an approximate system fragility function denoted UB^{appr}, assumed to follow a lognormal distribution, was estimated. This approximate system fragility is quantified by two parameters, namely, the lognormal mean and standard deviation, and denoted λ_{sys} and ζ_{sys}, respectively. The λ_{sys} and ζ_{sys} are determined from data generated using the actual *UB*. The geometric mean for the system, $\bar{\lambda}_{sys}$ is equal to the exponential of λ_{sys} and corresponds to a 50% probability of the system reaching or exceeding a selected ds_i. Table 9 summarizes the estimated parameters for UB^{appr} for the system damage states. The $\bar{\lambda}_{sys}$ values for $\Theta_{d,x}$ and $\Theta_{w,x}$ as the EDP are approximately 35%, 60%, and 16% smaller for multidirectional loading than for unidirectional loading for NLD, DS_I, and DS_{II}, respectively. The $\bar{\lambda}_{sys}$ values (Table 9) for $\Theta_{d,x}$ and $\Theta_{w,x}$ are much smaller than $\bar{\lambda}$ (Table 7) for each damage state due to the large dispersion in the component damage data noted previously, which implies more likely damage to the system (i.e., an SC-CLT wall) than an individual CLT wall panel corner (i.e., component) under lateral loading. For example, the $\bar{\lambda}$ values for DS_I (Table 7) show there is a 50% probability of reaching (or exceeding) a moderate damage state from the lower-bound system fragility or the component (corner) fragility at story drifts of about 2.3% and 1.3% for unidirectional and multidirectional loading, respectively, while the $\bar{\lambda}_{sys}$ values for DS_I (Table 9) show there is a 50% probability of reaching a moderate damage state from the upper-bound system fragility at much smaller story drifts of about 1.5% and 0.6% for unidirectional and multidirectional loading, respectively. Fig. 10 shows the system fragility functions for unidirectional (U) loading and multidirectional (M) loading. Two sets of UB fragility functions are shown; UB^{U} and UB^{M} from $1 - \prod_{i=1}^{m}[1 - P(F_{comp}|\text{EDP} = x)]$, and $\text{UB}^{\text{appr,U}}$ and $\text{UB}^{\text{appr,M}}$ from the estimated parameters in Table 9. The two upper-bound results are nearly identical. The results in Fig. 10 show that for a given $\Theta_{d,x}$ or $\Theta_{w,x}$, the probability of the system reaching or exceeding a selected ds_i is larger for multidirectional loading compared to unidirectional loading, consistent with previous observations that multidirectional loading

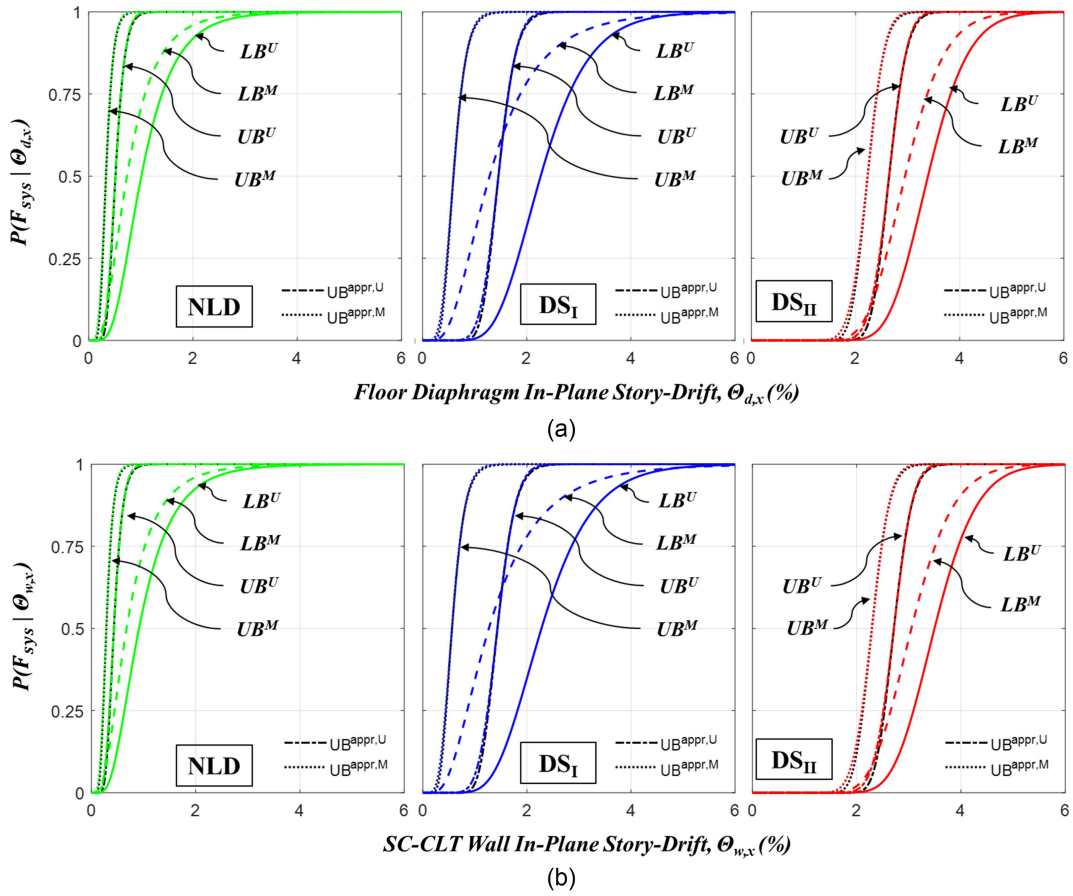

Fig. 10. LB and UB system fragilities with EDP as (a) $\Theta_{d,x}$; and (b) $\Theta_{w,x}$.

causes damage at smaller story-drift levels than unidirectional loading.

Summary and Conclusions

This paper presented an experimental study on the lateral-load response and damage of SC-CLT walls under multidirectional cyclic loading. The SC-CLT wall damage states are based on visual observations of SC-CLT walls tested in a 0.625-scale timber test subassembly. Four damage states were considered: (1) NLD; (2) DS_I; (3) DS_{II}; and (4) DS_{III}. NLD is an indistinguishable minor or cosmetic damage of the CLT wall panel that does not require any repair action. DS_I is a moderate damage where a simple repair action is needed. DS_{II} is a significant damage state where repair and/or strengthening of the CLT wall panel is required. DS_{III} is a severe damage state where the CLT wall panels are damaged to the extent that a 20% reduction in base shear resistance of the SC-CLT wall occurs. Three engineering demand parameters (EDPs) were used to quantify the SC-CLT wall damage states: (1) the floor diaphragm story drift; (2) the SC-CLT wall story drift; and (3) the CLT wall panel corner compression strain.

The lateral-load response and damage of two SC-CLT wall test specimens, one tested under unidirectional (in-plane) cyclic loading and the other tested under multidirectional (in-plane and out-of-plane) cyclic loading, were presented and compared. The test results show that multidirectional loading causes earlier damage (i.e., at smaller story-drift levels) to the SC-CLT wall panels than unidirectional loading. Predictions of the wall story drift associated with a damage state, made using closed-form-expressions (CFEs), were compared with the experimental results. The CFE results were relatively close to the experimental results for NLD and DS_I and conservative for DS_{II}.

For each damage state and for each EDP, two sets of sample data points (i.e., the EDP values for a given damage state) for the first observed damage at each wall panel corner were acquired [these data are given in Amer (2023)], one set from the unidirectional test and one set from the multidirectional test. The values of the EDPs in these data sets exhibit significant variability. Lognormal probability distributions were fit to the sample data. The lognormal mean of the population (for each EDP and damage state) was assumed to equal the lognormal mean for the sample data (for each EDP and damage state); however, the large and widely varying dispersion of the sample data (for the different EDPs and damage states) led to the use of Bayesian updating to estimate the population lognormal standard deviations (for each EDP and damage state).

Fragility functions for the damage states for an individual wall panel corner of an SC-CLT wall panel under compression (i.e., a component) and an entire SC-CLT wall (i.e., the system, including multiple wall panel corners) were developed from the test results. The fragility functions show that the probability of a CLT wall panel corner or an entire SC-CLT wall reaching or exceeding a damage state for a given story drift is larger when the wall is subjected to multidirectional loading than unidirectional loading.

In conclusion, simple observations from the cyclic lateral loading tests and the subsequent development of fragility functions demonstrate that multidirectional cyclic lateral loading of SC-CLT shear walls causes damage at smaller story-drift levels than

unidirectional loading. As a result, predictions of SC-CLT shear wall damage in buildings from earthquake ground motions using only unidirectional lateral loading test results are expected to underestimate the actual SC-CLT shear wall damage that will be caused by multidirectional building response. Future work on methods to mitigate potential damage to the corners of SC-CLT walls under multidirectional lateral loading is needed to fully achieve a low-damage lateral-load resisting system.

Data Availability Statement

All data that support the findings of this study are available from the corresponding author upon reasonable request.

Acknowledgments

This paper is based on work supported by a grant from the National Science Foundation (NSF), Award No. CMS-1635227, "Collaborative Research: A Resilience-Based Seismic Design Methodology for Tall Wood Buildings." The research reported in this paper was performed at the NHERI Lehigh Large-Scale Multi-Directional Hybrid Simulation Experimental Facility. Financial support for operating the NHERI Lehigh Experimental Facility was provided by the NSF under Cooperative Agreement Nos. CMMI-1520765 and CMMI-2037771. The authors are grateful for additional financial support provided by the Pennsylvania Infrastructure Technology Alliance and Lehigh University. The authors are grateful for the donations of products from SmartLam, Western Structures, Simpson Strong-Tie, and JVI used to construct the test specimens. The contributions of Professor Shiling Pei from the Colorado School of Mines, Professor J. Daniel Dolan from Washington State University, and the ATLSS Center staff are acknowledged. Any opinions, findings, and conclusions expressed in this paper are those of the authors and do not necessarily reflect the views of the National Science Foundation or others acknowledged here.

References

ACI (American Concrete Institute). 2007. *Acceptance criteria for special unbonded post-tensioned precast structural walls based on validation testing*. ACI ITG-5.1-07. Farmington Hills, MI: ACI.

Akbas, T. 2016. "Seismic response analysis of structures with nonlinear mechanisms using a modal approach." Ph.D. dissertation, Dept. of Civil and Environmental Engineering, Lehigh Univ.

Akbas, T., R. Sause, J. M. Ricles, R. Ganey, J. Berman, S. Loftus, J. D. Dolan, S. Pei, J. W. van de Lindt, and H.-E. Blomgren. 2017. "Analytical and experimental lateral-load response of self-centering posttensioned CLT walls." *J. Struct. Eng.* 143 (6): 04017019 https://doi.org/10.1061/(ASCE)ST.1943-541X.0001733.

Amer, A. 2023. "Multidirectional lateral-load testing of seismically resilient timber sub-assembly with SC-CLT wall, floor diaphragm, and gravity load system." Ph.D. dissertation, Dept. of Civil and Environmental Engineering, Lehigh Univ.

Amer, A., J. Ricles, and R. Sause. 2022. "Multi-directional cyclic response of self-centering cross-laminated timber shear walls." In *Proc., 12th National Conf. on Earthquake Engineering*. Salt Lake City: Earthquake Engineering Research Institute.

Ang, A. H.-S., and W. H. Tang. 2007. *Probability concepts in engineering—Emphasis on applications to civil and environmental engineering*. 2nd ed. Hoboken, NJ: Wiley.

APA—The Engineered Wood Association. 2016. *Product report: SmartLam cross-laminated timber*. PR-L319. Tacoma, WA: APA—The Engineered Wood Association.

APA—The Engineered Wood Association. 2019. *Standard for performance-rated cross laminated timber*. ANSI/APA PRG 320. Tacoma, WA: APA—The Engineered Wood Association.

Chiozzi, A., and E. Miranda. 2017. "Fragility functions for masonry infill walls with in-plane loading." *Earthquake Eng. Struct. Dyn.* 46 (15): 2831–2850. https://doi.org/10.1002/eqe.2934.

Dunbar, A. J. M., S. Pampanin, and A. H. Buchanan. 2014. "Seismic performance of core-walls for multi-storey timber buildings." In *Proc., NZSEE Conf.* Auckland, New Zealand: New Zealand Society of Earthquake Engineering.

Ganey, R., J. Berman, T. Akbas, S. Loftus, D. Dolan, R. Sause, J. Ricles, S. Pei, J. van de Lindt, and H.-E. Blomgren. 2017. "Experimental investigation of self-centering cross-laminated timber walls." *J. Struct. Eng.* 143 (10): 04017135 https://doi.org/10.1061/(ASCE)ST.1943-541X.0001877.

Iqbal, A., S. Pampanin, A. Palermo, and A. H. Buchanan. 2015. "Performance and design of LVL walls coupled with UFP dissipaters." *J. Earthquake Eng.* 19 (3): 383–409. https://doi.org/10.1080/13632469.2014.987406.

Kurama, Y., S. Pessiki, R. Sause, and L. W. Lu. 1999a. "Seismic behavior and design of unbonded post-tensioned precast concrete walls." *PCI J.* 44 (3): 72–89. https://doi.org/10.15554/pcij.05011999.72.89.

Kurama, Y., R. Sause, S. Pessiki, and L. W. Lu. 1999b. "Lateral load behavior and seismic design of unbonded post-tensioned precast concrete walls." *ACI Struct. J.* 96 (4): 622–632. https://doi.org/10.14359/700.

Lynch, S. M. 2007. *Introduction to applied Bayesian statistics and estimation for social scientists*. New York: Springer.

Mercan, O., J. M. Ricles, R. Sause, and T. Marullo. 2009. "Kinematic transformations for planar multi-directional pseudodynamic testing." *Earthquake Eng. Struct. Dyn.* 38 (9): 1093–1119. https://doi.org/10.1002/eqe.886.

Moroder, D., S. Pampanin, A. Palermo, T. Smith, F. Sarti, and A. Buchanan. 2017. "Diaphragm connections in structures with rocking timber walls." *Struct. Eng. Int.* 27 (2): 165–174. https://doi.org/10.2749/101686617X14881932435574.

Palermo, A., S. Pampanin, and A. Buchanan. 2006. "Experimental investigation on LVL seismic resistant wall and frame subassemblies." In *Proc., First European Conf. on Earthquake Engineering and Seismology*. Geneva: European Association for Earthquake Engineering.

Pei, S., J. W. van de Lindt, A. R. Barbosa, J. W. Berman, E. McDonnell, J. D. Dolan, H.-E. Blomgren, R. B. Zimmerman, D. Huang, and S. Wichman. 2019. "Experimental seismic response of a resilient 2-story mass-timber building with post-tensioned rocking walls." *J. Struct. Eng.* 145 (11): 04019120. https://doi.org/10.1061/(ASCE)ST.1943-541X.0002382.

Perez, F. J., R. Sause, and S. Pessiki. 2007. "Analytical and experimental lateral load behavior of unbonded posttensioned precast concrete walls." *J. Struct. Eng.* 133 (11): 1531–1540. https://doi.org/10.1061/(ASCE)0733-9445(2007)133:11(1531).

Ross, R. J. 2010. *Wood handbook: Wood as an engineering material*. Madison, WI: US Dept. of Agriculture, Forest Service, Forest Products Laboratory.

Sause, R., J. Ricles, A. Amer, and T. Marullo. 2020. "Multi-directional cyclic testing of cross-laminated timber rocking wall-floor diaphragm sub-assemblies." In *Proc., 17th World Conf. on Earthquake Engineering*. Sendai, Japan: WCEE2020 Local Organization Committee.

Seo, C. Y., and R. Sause. 2005. "Ductility demands on self-centering systems under earthquake loading." *ACI Struct. J.* 102 (2): 275–285. https://doi.org/10.14359/14279.